Microchimica Acta (2019) 186: 675
https://doi.org/10.1007/s00604-019-3762-5

ORIGINAL PAPER

One-step synthesis of N-doped carbon dots, and their applications in curcumin sensing, fluorescent inks, and super-resolution nanoscopy

Lingli Bu[1] · Tao Luo[1] · Huanjun Peng[2] · Ling Li[1] · Dengying Long[2] · Jingdong Peng[2] · Jing Huang[1]

Received: 24 March 2019 / Accepted: 14 August 2019 / Published online: 7 September 2019

Abstract

Nitrogen-doped carbon dots (N-CDs) with fluorescence excitation/emission maxima at 365/450 nm were prepared by a one-step hydrothermal approach. The dots possess remarkable photostability, fluorescence blinking and good biocompatibility, and this favors utilization in stochastic optical reconstruction microscopy (STORM). A spatial resolution down to ~60 nm was achieved when imaging HeLa cells using 647-nm laser excitation. This opens new possibilities for various super-resolution techniques based on stochastic optical switching. The remarkable optical properties of the N-CDs also enable them to be applied as invisible security ink for use in patterning, information storage and anti-counterfeiting. Further, it is found that the fluorescence of the N-CDs can be quenched by curcumin with high efficiency due to a combination of inner filter effect and static quenching. Based on this, a fluorometric assay with a detection limit of 21 ng mL^{-1} was developed for the determination of curcumin.

Keywords Carbon dots · Blinking · Super-resolution imaging · Fluorescent ink · Cell imaging · Fluorescence detection · Curcumin

Introduction

The spatial resolution for optical microscopy is limited by classic optical diffraction (Abbe's diffraction limit), which brings physical challenges to acquisition of accurate information of the images [1]. Fortunately, this seemingly impenetrable barrier has been shattered by the rapid development of super-resolution imaging techniques and the resolution has been improved by an order of magnitude [2]. Selection of fluorescent probes is a key factor for the realization of super-resolution techniques. A large number of fluorescent probes including fluorescent proteins (FPs) [3], organic dyes [4] and quantum dots (QDs) [5] have been exploited for super-resolution imaging. However, FPs and organic dyes suffer from insufficient brightness and low photostability, which have restricted their use for observation over a long duration [6, 7]. In contrast, QDs are brighter at the single-molecule level, possess good stability against photobleaching and exceptional photophysical properties [8], placing them in an advantageous position. Nevertheless, the potential cytotoxicity of semiconductor quantum dots needs to be taken into consideration because of toxic heavy metals.

As a new class of carbon nanomaterial, CDs have attracted considerable attentions since their first discovery [9]. Until now, numerous synthetic methods of CDs have been developed [10, 11]. Among them,

Lingli Bu and Tao Luo contributed equally to this work.

Electronic supplementary material The online version of this article (https://doi.org/10.1007/s00604-019-3762-5) contains supplementary material, which is available to authorized users.

✉ Jingdong Peng
hxpengjd@swu.edu.cn

✉ Jing Huang
huangjing16@hnu.edu.cn

[1] Institute of Chemical Biology and Nanomedicine (ICBN), State Key Laboratory of Chemo/Biosensing and Chemometrics, College of Chemistry and Chemical Engineering, College of Biology, Hunan Provincial Key Laboratory of Biomacromolecular Chemical Biology, Hunan University, Changsha 410082, People's Republic of China

[2] College of Chemistry and Chemical Engineering, Southwest University, Chongqing 400715, People's Republic of China

hydrothermal treatment of various natural bio-precursors has been one of the most common methods due to the advantages of simplicity and low cost. However, a great number of these CDs have the flaws of low quantum yield (QY) and restricted active sites, restricting their widespread applications. Doping CDs with heteroatoms (nitrogen, phosphorus, sulfur, etc.) is deemed to be a valid strategy to address this issue by modulating their intrinsic properties, improving their fluorescent properties and quantum yield [12, 13]. Of these, doping of electron-rich N atoms is the most common type and the doping level has some relativity with quantum yield [14]. CDs have become a very promising nanomaterial in the area of sensors, optoelectronic devices, nanomedicine and bioimaging due to their fascinating properties including good aqueous solubility, high photostability, super biocompatibility, low toxicity, etc. [15–17]. Additionally, recent studies have suggested that CDs exhibit fluorescence blinking (intermittency or bright/dark transition) [18]. The property is beneficial for being used as photoswitchable probes in stochastic optical reconstruction microscopy (STORM). For conventional photoswitchable dyes, the acquisition of super-resolution images typically relies on multiple illumination lasers for bleaching and reactivation or toxic buffer to encourage photoswitching [19]. CDs, however, need not be photoactivated due to the inherent fluorescence blinking and only one single laser is required, suggesting that CDs are promising candidates for super-resolution imaging.

Here, we synthesized nitrogen-rich CDs (N-CDs) through one-step hydrothermal treatment of chrysanthemum buds and ethylenediamine. Xu et al. prepared nitrogen-doped C-dots using tribute chrysanthemum as precursors [20]. Comparison showed that our newly synthesized N-CDs exhibited great quantum yield (28.5%) by introducing ethylenediamine as the doping nitrogen agent. We have succeeded in exploiting the fluorescence blinking behavior of N-CDs for STORM imaging. Single-particle measurements showed the N-CDs had appealing features of high photostability and robust fluorescence fluctuation. We further achieved high-precision optical reconstruction imaging of HeLa cells and DNA fibers with a full-width half-maximum (fwhm) of ~59.5 nm. We observed that the fluorescence of N-CDs was highly sensitive to curcumin, which is extracted from turmeric and has been widely used in food spice, medical industry, clinical therapy, etc. [21]. Hence the N-CDs were applied as curcumin sensors based on the IFE and SQE (Scheme 1). Additionally, due to remarkable fluorescence properties, excellent stability and transparency under ambient light, N-CDs were also suitable as invisible security ink for anti-counterfeiting and information encryption.

Experimental

Materials and apparatus

Ethylenediamine (EDA) and curcumin were purchased from Aladdin Reagent Co., Ltd. (Shanghai, China, https://www.aladdin-e.com/). Dialysis bag (MWCO 1000 Da) was obtained from Yuanye Biotechnology Co., Ltd. (Shanghai, China, http://www.shyuanye.com/). Anti-ds DNA antibody (ab27156) was from Abcam Inc. (Cambridge, UK, http://www.abcam.cn/). Goat serum and bovine serum albumin (BSA) were purchased from Beyotime Biotech Co., Ltd. (Shanghai, China, https://www.beyotime.com/). Chrysanthemum buds were procured from Yonghui Supermarket (Chongqing, China). HeLa cells were obtained from Molecular Science and Biomedicine Laboratory, Chemistry and Chemical Engineering, Hunan University.

High resolution transmittance electron microscopy (HRTEM) images of N-CDs were obtained from a FEI-Tecnai G2 F20 S-Twin (FEI, US, 200 kV). Atomic force microscopy (AFM) measurements were performed using a Bruker Dimension Icon AFM micro-scope (Bruker, Germany). X-ray diffraction (XRD) patterns of N-CDs were recorded on a Shimadu XRD-6100 powder X-ray diffractometer. X-ray photoelectron spectroscopy (XPS) spectra were performed on K-Alpha$^+$ spectrometer (Thermo Fisher Scientific, UK). UV–vis and fluorescence spectra were obtained from the UV–3600 spectrophotometer (Hitachi, Japan) and F-2500 fluorescence spectrophotometer (Hitachi, Japan), respectively. Zeta potential was measured on a Malvern Zetasizer Nano ZSP. FL-TCSPC Fluorolog-3 spectrometer (Horiba Jobin Yvon Inc., France) was applied for fluorescence lifetime measurements. Cytotoxicity evaluation was conducted using an ELISA reader (Spark 10 M, Tecan, Switzerland). Bioimaging was performed on a Nikon A1 confocal laser scanning microscope (CLSM) (Nikon Instruments, Tokyo, Japan).

Synthesis and purification of N-CDs

The N-CDs were synthesized as follows: 0.5 g dried chrysanthemum buds, 100 μL ethylenediamine and 20 mL deionized water were added into a 50 mL steel-lined autoclave and heated to 180 °C for 6 h. The solution changed from primrose yellow to dark brown. After cooling down to room temperature, the obtained solution was centrifuged at 8000 rpm for 15 min, the supernatant was adjusted to neutral with diluted HCl and purified using 0.22 μm filtration membrane. Subsequently, the product solution was further purified in a dialysis bag (1000 MWCO) to remove the non-reacted materials. Deionized water was replaced every few hours during this procedure. Then, N-CDs solution was lyophilized and dispersed in deionized water as stock solution (4 mg mL^{-1}).

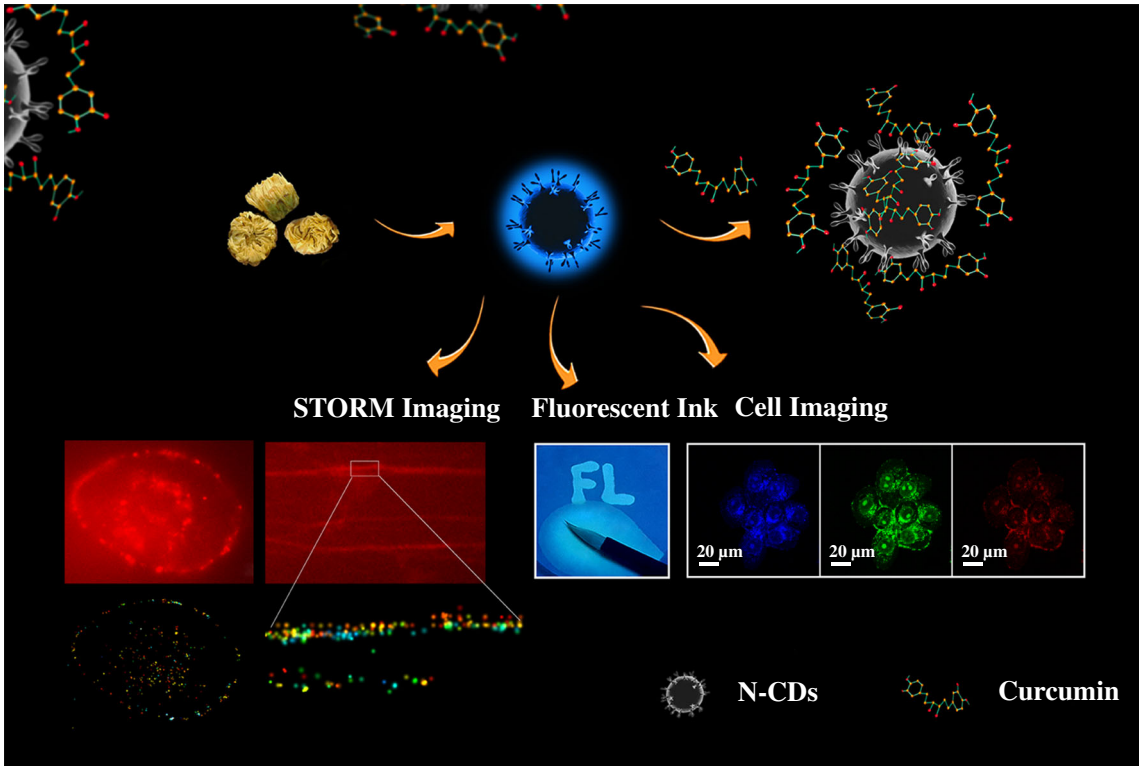

Scheme 1 Schematic illustration of the preparation and versatile applications of N-CDs

Fluorescent detection of curcumin

Stock solution of curcumin was prepared in dimethyl sulfoxide and stored in the dark. In a typical experiment, 2.0 mL BR buffer (40 mM, pH 6.0), 100 μL N-CDs solution (4 mg mL^{-1}), serial concentrations of curcumin (final concentration of 0–40 μg mL^{-1}) were mixed thoroughly and diluted to 10 mL using deionized water. After equilibration for 2 min, the fluorescence spectra were recorded under the excitation wavelength of 365 nm (λ_{em} = 450 nm, scan rate 12,000, 1 cm quartz cuvette). The excitation and emission slit widths were both set as 10 nm.

Super-resolution imaging of HeLa cells and DNA fibers

HeLa cells used in the wide-field cellular imaging were also applied for super-resolution imaging with 647 nm laser excitation. DNA fibers were obtained through the DNA spreading technique [22]. HeLa Cells were spotted onto the surface of a glass slide and lysed in spreading buffer (50 mM EDTA, 0.5% SDS in 200 mM Tris-HCl, pH 7.5). Then the slide was tilted and dried naturally. Then the slide was immersed in 3:1 methanol/acetic acid for 10 min and incubated in 2.5 M HCl for 45 min. Then it was neutralized in 0.4 M Tris-HCl (pH 7.5) for 5 min and washed in 10 mM phosphate buffered saline (PBS, containing 0.138 M NaCl, 0.0027 M KCl, pH 7.4) for three times. The slide was incubated with 100 μL of anti-ds DNA antibody solution (1:1000 dilution in PBS with 5% BSA, 10% goat serum) and covered with a piece of sealing film to ensure the solution covered the entire glass surface. After incubated in a humidor for 1 h, the slide was washed in PBST buffer (PBS containing 0.1% Tween 20) for 10 min and incubated with diluted N-CDs solution. After washing with PBST, imaging was carried out by 647 nm illumination (100X, 1.49 NA, frame rate: 10 MHz, the field of view: 512 × 512 pixels).

The detailed information of quantum yield measurement, electrochemistry of N-CDs, procedure for curcumin sensing in real samples, cytotoxicity assay and single particle study were shown in the Supporting Material.

Results and discussion

Characterization of N-CDs

The morphology and structure of the N-CDs were characterized by TEM. Figure 1a shows that the N-CDs are well monodispersed and uniformly spherical. The particle size distribution of N-CDs (fifty particles) is mainly in the range of 1.7–3.3 nm with an average size of ~2.7 nm (Fig. 1a, inset). The HRTEM image (Fig. 1b) clearly shows the graphite-like crystalline structure of N-CDs with a lattice spacing of

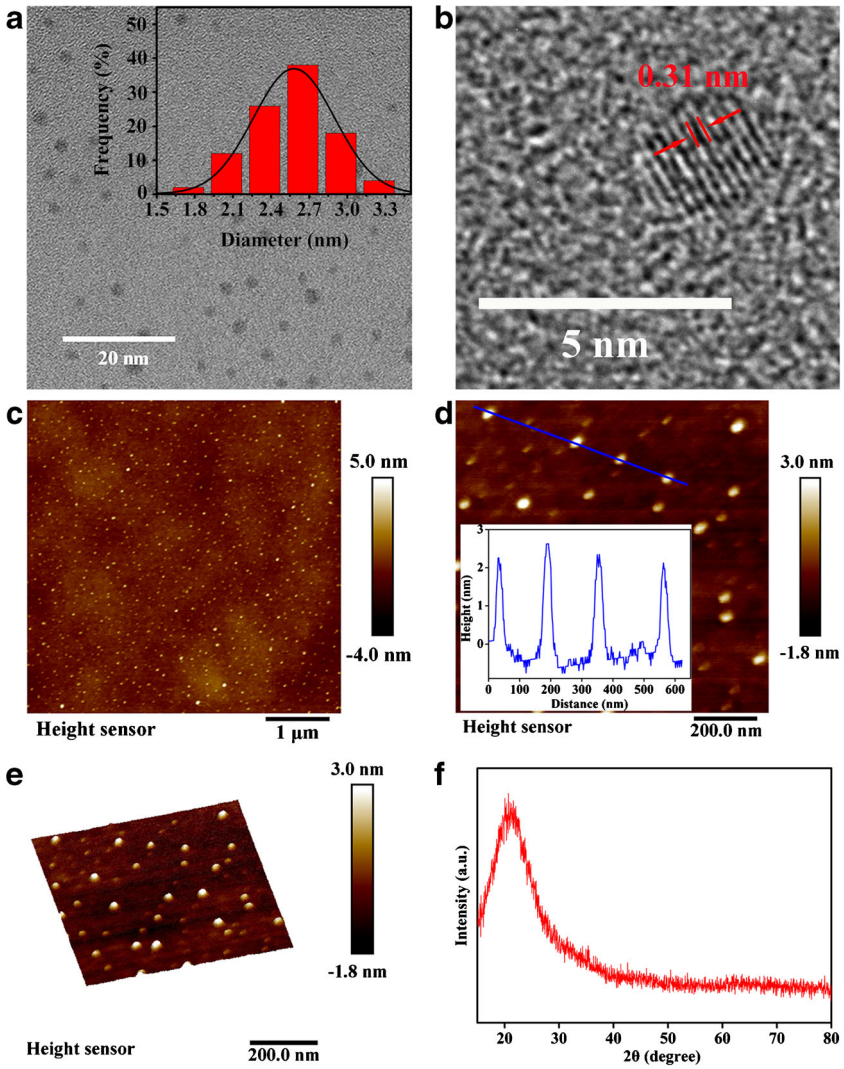

Fig. 1 **a** TEM and (**b**) HRTEM images of N-CDs. Inset: the corresponding size distribution histogram. **c** AFM image of N-CDs (1 μm) and (**d**) extracted profile (200 nm). Inset: height profile along the line. **e** Three-dimensional diagram of N-CDs (corresponding image of d). (**f**) XRD pattern of N-CDs

0.31 nm, which is consistent with the (002) facet of graphite [23]. AFM measurements were performed to reveal the particle height distribution (z-profile). Homogeneous and tiny N-CDs are formed and no aggregation is observed (Fig. 1c, d). The cross-sectional view of the nanoparticles suggests that the average thickness of N-CDs is ~2.3 nm (Fig. 1d, inset). Three-dimensional image of N-CDs corresponding two-dimensional images of Fig. 1d is observed (Fig. 1e). The XRD pattern of N-CDs (Fig. 1f) displays a broad diffraction peak at 2θ = 21.4°, associated with the (002) plane of typical graphitic structure [24], which further confirmed the results of HRTEM image. The broadening of the diffraction peak resulted from the small size of N-CDs [25].

Next, surface groups and elemental analysis of the N-CDs were characterized by XPS and FTIR spectra. The FT-IR spectrum (Fig. 2a) shows the characteristic absorption bands of O–H and N–H stretching vibrations at 3357 cm^{-1}, C–H, C–N, C=O and C=C stretching vibrations at 2921, 2053, 1634 and 1602 cm^{-1}, respectively. The peak at 1507 cm^{-1} is corresponded to the N–H bending vibration, bands at 1341 and 1034 cm^{-1} correspond to C–O–C asymmetric stretching vibration and symmetrical stretching vibration. XPS (Fig. 2b) spectrum exhibits three main peaks at 283.8, 397.6 and 530.3 eV, which are assigned to the C 1 s, N 1 s and O 1 s, respectively. The relative elemental contents are 67.22% of C, 18.01% of N and 14.77% of O, respectively. The high-resolution spectrum of C 1 s exhibits four peaks at 287.86, 286.02, 285.12 and 284.69 eV, which can be attributed to C=O, C–N, C–C/C=C and C–O bonding, respectively (Fig. 2c). The N 1 s spectrum (Fig. 2d) indicates that nitrogen exists in the form of N–H (401.53 eV), N–C (401.01 eV) and C–N–C (399.50 eV). The O 1 s spectrum (Fig. 2e) can be subdivided into three separated peaks that correspond to C–OH/C–O–C (531.11 eV), O–H (532.29 eV) and C=O (532.50 eV) functional groups. The XPS data indicated that the N-CDs were carbon-rich with nitrogen and oxygen, agreeing with the FT-IR analysis. The zeta potential of N-CDs in neutral solution is −8.67 mV (Fig. 2f), suggesting that the surface of N-CDs is functionalized with oxygen-rich groups (carboxyl and hydroxyl groups). All these abundant functional

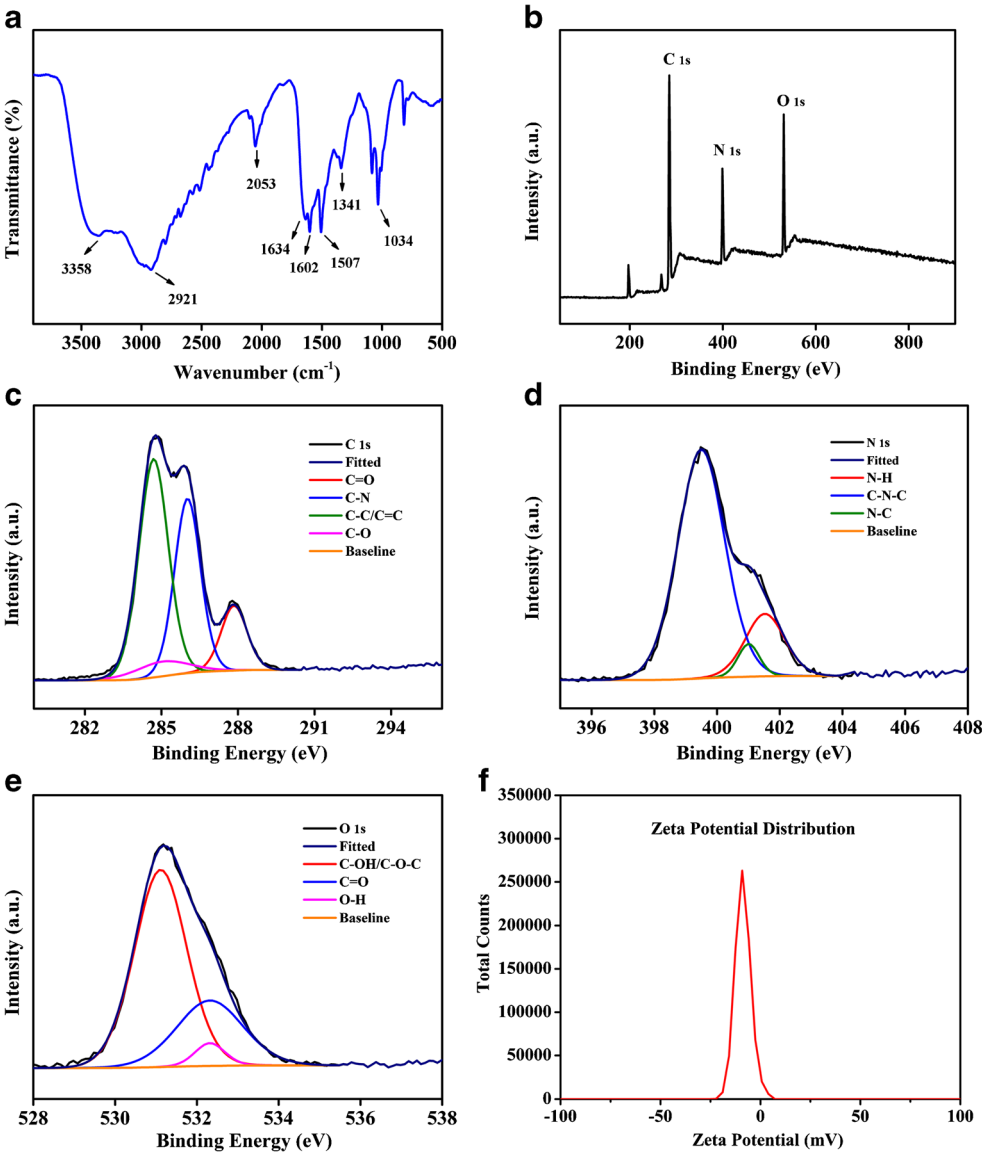

Fig. 2 **a** FTIR spectrum of N-CDs. **b** XPS pattern of N-CDs. High-resolution XPS spectra of (**c**) C 1 s peak, (**d**) N 1 s peak and (**e**) O 1 s peak. **f** Zeta potential of N-CDs

groups enhanced the hydrophilicity and stability of N-CDs in aqueous solution, which were crucial for their future applications in bioimaging and sensing.

Optical properties of N-CDs

UV–vis absorption and fluorescence (FL) spectra of the N-CDs solution are depicted in Fig. 3a. The N-CDs solution displays two intense absorption peaks at 240 and 342 nm, which are due to the π–π^* transition of sp^2 carbon and n–π^* transition of the C=O bond [26]. The N-CDs exhibit a maximum emission peak at 450 nm upon 365 nm excitation and emit bright blue-green fluorescence illuminated by 365 nm UV (Fig. 3a, inset). Figure 3b shows an excitation-dependent fluorescence behavior, which is considered one of the most distinct characteristics of numerous fluorescent quantum dots and may be attributed to the size inhomogeneity and multiple surface trapping states [27]. The unique feature made them emit multicolor fluorescence under different excitation wavelengths, and particularly benefit for optical bioimaging. The QY of N-CDs was calculated to be 28.5% with quintile sulfate as a reference (Fig. S1 and Table S1). Additionally, the fluorescence stability of N-CDs was explored. The results show the fluorescence intensity of N-CDs solution remains stable under continuous UV exposure (Fig. S2a). No significant fluorescence intensity changes are displayed with the increase of ionic strength (Fig. S2b). The concentration of N-CDs, is also optimized (Fig. S2c). As the N-CDs concentration increase, the fluorescence intensity enhances until 40 μg mL^{-1}. Due to the aggregation of N-CDs, the fluorescence decreased gradually at the concentration higher than 40 μg mL^{-1}. As shown in Fig. S2d, the

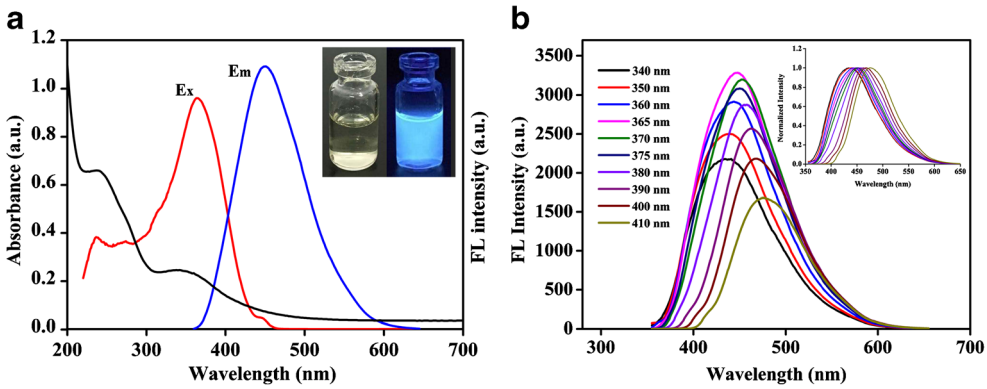

Fig. 3 **a** UV–vis absorption and fluorescence spectra of N-CDs. Inset: images of N-CDs under visible light (left) and 365 nm UV light (right). **b** Fluorescence emission spectra of N-CDs under various excitation wavelengths from 340 nm to 410 nm. (Inset: normalized fluorescence spectra)

fluorescence intensity of N-CDs almost keep stable within the pH range of 5.5–8.0, indicating the N-CDs are stable in physiological solution. Taken together, the N-CDs possess excellent optical stability in physiological condition, which fully highlights their high feasibility for nanoprobe.

Fluorescence detection of curcumin and its possible sensing mechanism

It has been reported that curcumin has multi-effect physiological activities including anti-cancer, antimicrobial, *etc* [28]. Given the critical role of curcumin in the medical industry and clinical therapy, the quantification of curcumin has attracted much attention. Currently, a variety of sensing strategy for curcumin has been developed. In this study, we found the N-CDs had a high-sensitive response to curcumin. The sensitivity of the N-CDs nanosensor toward curcumin was evaluated under optimized conditions (at pH 6.0 with 40 μg mL^{-1} of N-CDs). The fluorescence intensity of N-CDs decreases gradually with the increment of curcumin (Fig. 4a). Figure 4b shows that the quenching efficiency (F_0/F) is linearly dependent upon the concentration of curcumin at lower levels (0.2–8.0 μg mL^{-1}), where F_0 and F are the fluorescence intensity of N-CDs in the absence and presence of curcumin, respectively. The limit of detection (LOD), based on 3*S*/*K*, is calculated to be 20.81 ng mL^{-1} (based on 3*S*/*K*). A performance comparison of the proposed method with other reported methods is shown in Table S2. The results indicated that this proposed strategy can exhibit much better or comparable performances in the respects of simplicity, sensitivity, cost, etc.

Selectivity is a critical parameter for evaluating the specificity of probes. Here, we investigated the effect of various interfering substances on the determination of curcumin, including some common metal ions (K^+, Na^+, NH_4^+, Fe^{2+}, Mg^{2+}, Ca^{2+}, Zn^{2+}, Mn^{2+}, Fe^{3+}, Co^{2+}, Ni^{2+}), sugars and amino acids (glucose, sucrose, fructose, L-phenylalanine, L-tyrosine, L-arginine, L-lysine, L-glycine, L-serine, L-glutamic acid), and drugs (curcumin, morin, kaempferol, doxorubicin, tetracycline, rutin, ofloxacin). As shown in Fig. 4c, it is evident that the fluorescence quenching of N-CDs caused by curcumin (20 μg mL^{-1}) is much more obvious than others (200 μM). The coexistence of various interferents has negligible influence on the detection system, and this strongly verified N-CDs probe had excellent selectivity for curcumin. In order to access the feasibility and practicality of this approach, N-CDs were further applied for the detection of curcumin in human urine samples from volunteers spiked with curcumin

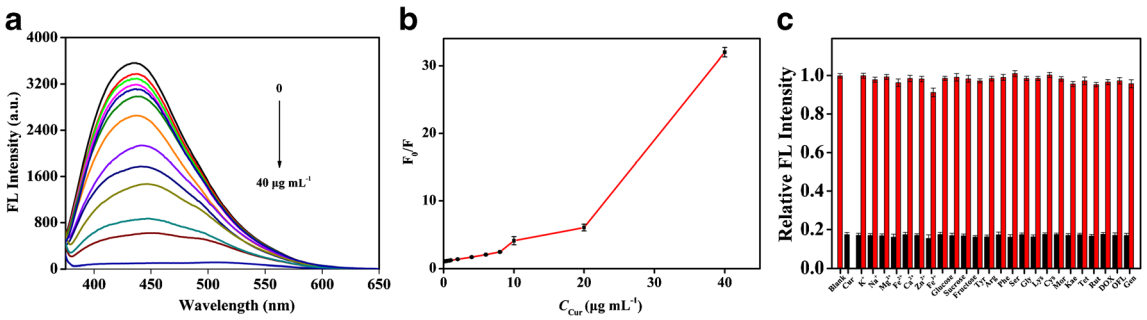

Fig. 4 **a** Fluorescence spectra of N-CDs in the presence of various concentrations of curcumin (λ_{ex} = 365 nm, λ_{em} = 450 nm). **b** Linear relationship of F_0/F versus curcumin concentration (0.2–8.0 μg mL^{-1}). Inset: Plot of F_0/F versus curcumin. **c** Selectivity of curcumin detection. Red bars show the fluorescence intensity of N-CDs in the presence of other interferents. Blank bars show the following addition of curcumin into the previous solutions

(see Supporting Material). As listed in Table S3, high average spiked recoveries with low RSD in the range of 0.96–3.06% indicated that the proposed sensing platform for analyzing trace amounts of curcumin was accurate and reliable.

To reveal the quenching mechanism of N-CDs for curcumin sensing, spectra analysis and fluorescence lifetime assay were performed. As shown in Fig. 5a, curcumin has a broad absorption peak in the wavelength range of 300–550 nm, the excitation and emission spectra of N-CDs have quite plenty of overlap with the UV–vis absorption of curcumin, thus the quenching may be related to IFE or fluorescence resonance energy transfer (FRET) [29]. In the meanwhile, the coexistence of other mechanisms may also occur. Generally, fluorescence quenching usually results from the static quenching effect (SQE) or dynamic quenching effect (DQE) or simultaneously [30]. Both DQE and SQE through ground-state complex formation model can be described by the Stern–Volmer equation: [30]

$$F_0/F = 1 + K_{SV}\, c_q = 1 + K_q \tau_0\, c_q$$

Here, F_0 and F are the fluorescence intensity in the absence and presence of the quencher, K_{SV} is the quenching constant, τ_0 is the average lifetime of N-CDs (9.28 ns) and K_q is the quenching rate constant. For curcumin sensing, Ksv = 6.37 × 10^4 M^{-1}, K_q is calculated to be 6.86 × 10^{12} M^{-1} s^{-1}. The resulted K_q is much higher than the maximum scatter collision quenching constant (1.0 × 10^{10} M^{-1} s^{-1}) [30], suggesting a static quenching.

For further proof, fluorescence lifetime assay was carried out. Decay spectra are shown in Fig. 5b, the average fluorescence lifetime values are calculated as 9.28 ns and 9.44 ns in the absence and presence of curcumin (Table S4), implying that FRET in the quenching of N-CDs is ruled out. Next, the energy levels of the highest occupied molecular orbital (E_{HOMO}) and lowest unoccupied molecular orbital (E_{LUMO}) of N-CDs were investigated through the combination of cyclic voltammetry (CV) and UV–vis spectra. The values were estimated based on the empirical formula [31].

$$E_{HOMO}(eV) = -(E_{ox} + 4.4)$$
$$E_{LUMO}(eV) = -(E_{red} + 4.4)$$

Where E_{ox} is the onset of oxidation potential of N-CDs and E_{red} is the reduction potential. E_{red} is measured to be −0.52 eV from the cyclic voltammogram (Fig. 5c) and the blank analysis is shown in Fig. S3. Therefore, the value of E_{LUMO} is −3.88 eV, but the E_{HOMO} value is unavailable to obtain due to the irreversibility of the oxidation behavior. The HOMO energy level can be calculated by the combination of E_{LUMO} and the optical energy band gap [32] (E_g, the absorption edge in the optical data)

$$E_{HOMO} = E_{LUMO} - E_g$$

E_g is determined as 3.96 eV from the Tauc plot curve demonstrated in Fig. S4. Thus, the E_{HOMO} value of N-CDs is −7.84 eV. The calculated ELUMO and EHOMO of curcumin are −3.16 eV and − 5.06 eV respectively. This made the

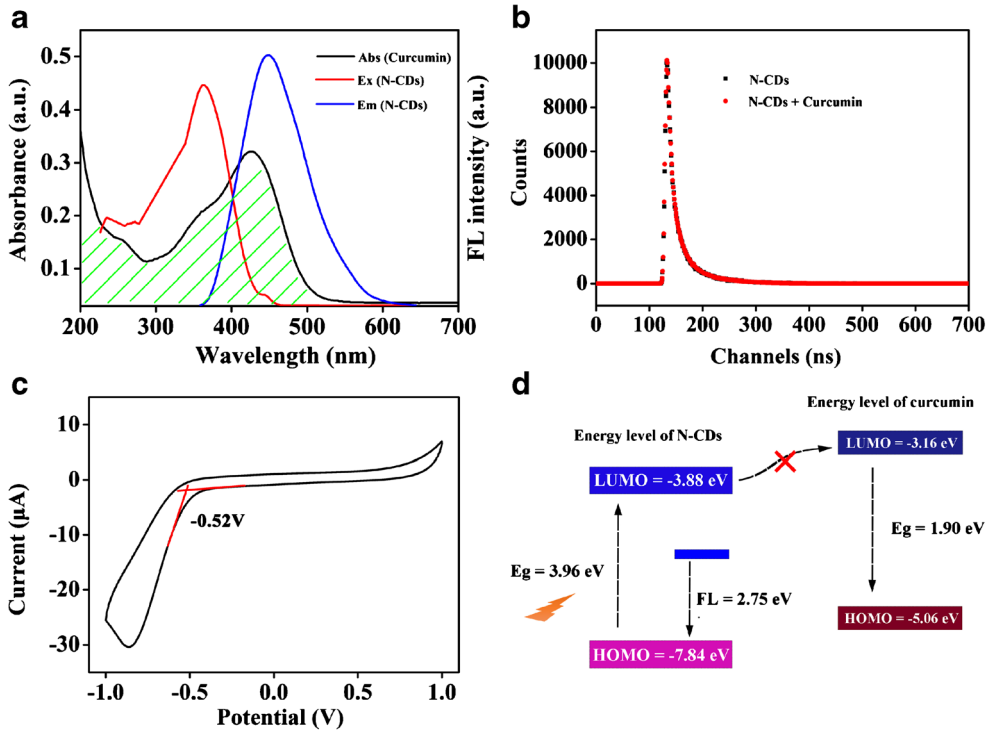

Fig. 5 **a** The spectral overlap between the absorption spectrum of curcumin and the excitation emission spectra of N-CDs. **b** Decay curves of N-CDs in the absence and presence of curcumin. **c** Cyclic voltammetry curve of N-CDs (scan rate: 50 mV s^{-1}). **d** Energy diagram of N-CDs and curcumin

electron transfer from the LUMO of N-CDs to the LUMO of curcumin impossible (Fig. 5d). Therefore, a combined effect of IFE and SQE may be responsible for curcumin-induced fluorescence quenching process.

Fluorescence security ink

CDs have versatile application due to their unique optical characteristics. Beyond the fluorescence detection of curcumin, the water-soluble N-CDs can be employed as a new kind of fluorescence security ink. The ink might be used in information storage and advanced anti-counterfeiting due to their remarkable fluorescence properties. The images on the filter paper are displayed in Fig. 6a. The patterns which are invisible under ambient light and glow brightly exposed to UV light, ensuring the security of the load information. The labeled patterns still remained good stability after several-months storage under ambient temperature. Compared with traditional inks, the new type of CDs ink is clear, permanent and pollution-free.

Super-resolution nanoscopy application

As state above, the N-CDs possessed good optical properties in physiological condition. This inspired us to investigate the feasibility of N-CDs for cellular imaging. The cytotoxicity study shows N-CDs have low toxicity, excellent biocompatibility for cell imaging (Fig. S5a). The confocal images of Hela cells treated with N-CDs (40 μg mL^{-1}) show multicolor fluorescence including blue, green, and less red with different excitation wavelengths (Fig. 6b). The bright-field image displays clear cell contour and no morphology change after the treatment of N-CDs, suggesting the N-CDs is a promising candidate for bioimaging.

CDs have been reported to behave fluorescence blinking with a great potential application in super-resolution techniques [33]. We investigated the fluorescence blinking effect and photon budgets of N-CDs adsorbed on a surface with TIRF microscopy (see Supporting Material for details). Figure 6c shows several typical examples of fluorescent time traces of

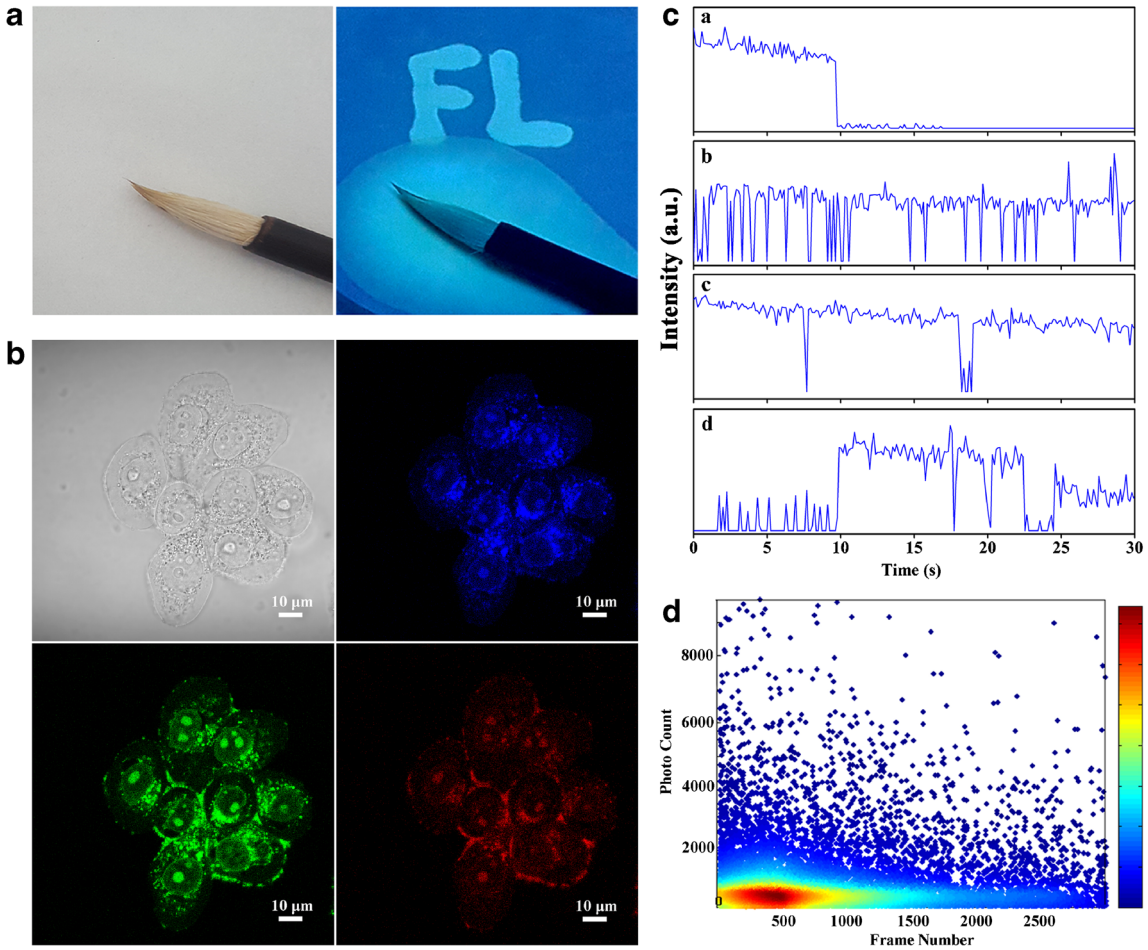

Fig. 6 **a** Fluorescent ink application of N-CDs. **b** Bright field and fluorescent images of HeLa cells incubated with N-CDs at the excitation wavelengths of 405 nm, 488 nm, and 561 nm, respectively. Scale bar: 10 μm. **c** Fluorescence time traces and (**d**) Photon counts statistics of individual N-CDs

individual N-CDs. These can be roughly divided into two categories: one was single-step blinking which exhibits a high-intensity on-state and single-step bleaching, the other was multi-step blinking. The single-step on-off transition (time trace a) indicated that the emission come from a single chromophore or highly coupled multi-chromophores rather than the stack of fluorescence signals from several particles [18]. As for multi-step blinking, a random subset of N-CDs was activated to the on-state and then deactivated to a reversible off-state, this multi-state fluorescence phenomenon has been reported in a variety of CDs [34]. Figure 6d shows the photon count distribution and the average photon budgets are calculated to be around 900 irradiated by 647 nm laser without any external additives, ensuring the high location accuracy in super-resolution imaging. The photostability measurement of individual N-CDs demonstrates that individual CDs have high resistance to photobleaching (Fig. S5b).

On the basis of these results above, we ask if N-CDs had the ability for super-resolution localization. N-CDs were directly spin coated on a clear coverslip, irradiated by the 647 nm laser light, the fluorescent spots were constantly identified and then localized. Figure 7a shows the traditional wide-field confocal image and Fig. 7b is the high-precision optical reconstruction image of the single-molecule diffraction limited spots. By comparison, it was apparent that the reconstructed image revealed striking difference in the degree of detail, spatial resolution and signal-to-background ratio were remarkably enhanced. The intensity profiles of the magnified region (Fig. 7c, circle 1) are shown in Fig. 7d, the average localization precision for single N-CDs fitted with a Gaussian distribution is ~38 nm (approximately 8.86-fold enhancement). Figure 7e shows a representative cross-section of two closely-spaced spots (circle 2), indicating that two spots separated by a distance of ~67.5 nm might be distinguished from each other.

Next, we applied the N-CDs for the super-resolution imaging of HeLa cells and DNA fibers (see Supporting Information for details). As can be seen in Fig. 8b, d, reconstructed images provide clearer contour, more specific details and lesser background noise compared with the diffraction-limited image (Fig. 8a, c). The mechanism of the immunofluorescence staining of the DNA fibers using N-CDs is not entirely clear at present and this awaits future studies. An average localization precision of ~66.5 nm is achieved by plotted the intensity profiles, which is nearly 10.11-fold resolution

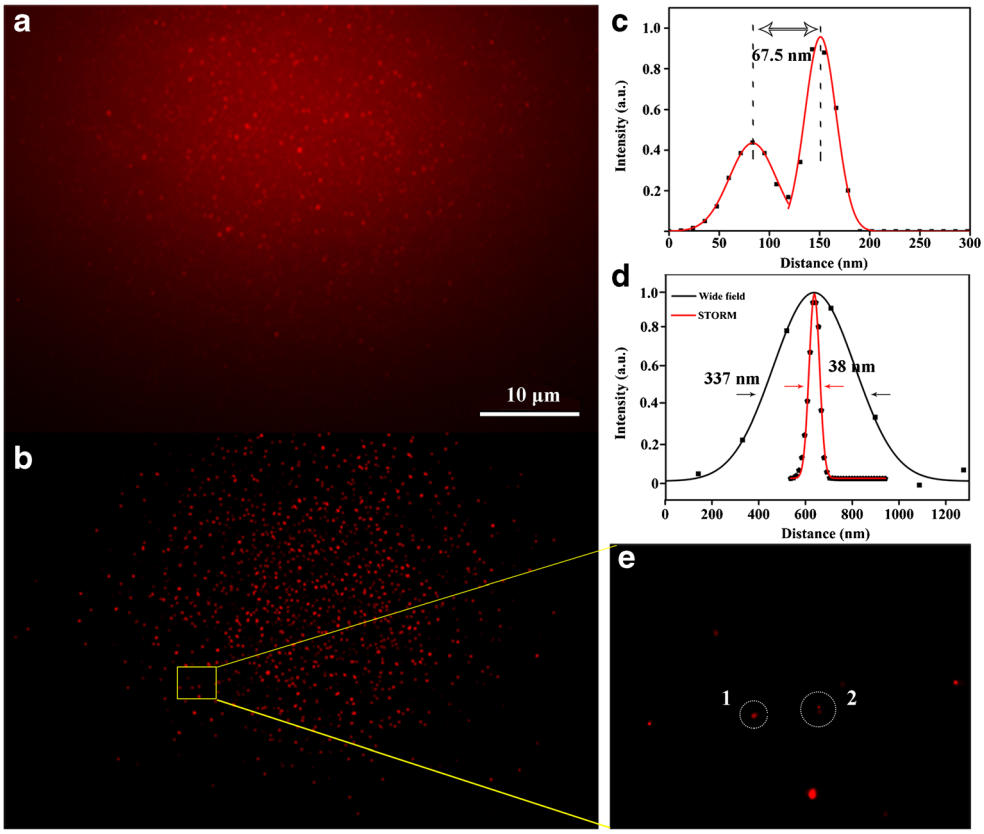

Fig. 7 Single-molecule localization analysis of N-CDs. **a** Wide-field image of spin-coated N-CDs. **b** STORM analysis of raw data from panel a. **c** Magnified region in yellow box of panel b. **d** Comparison of wide-field and STORM intensity profiles of circle 1. **e** The intensity profile of two adjacent spots in circle 2

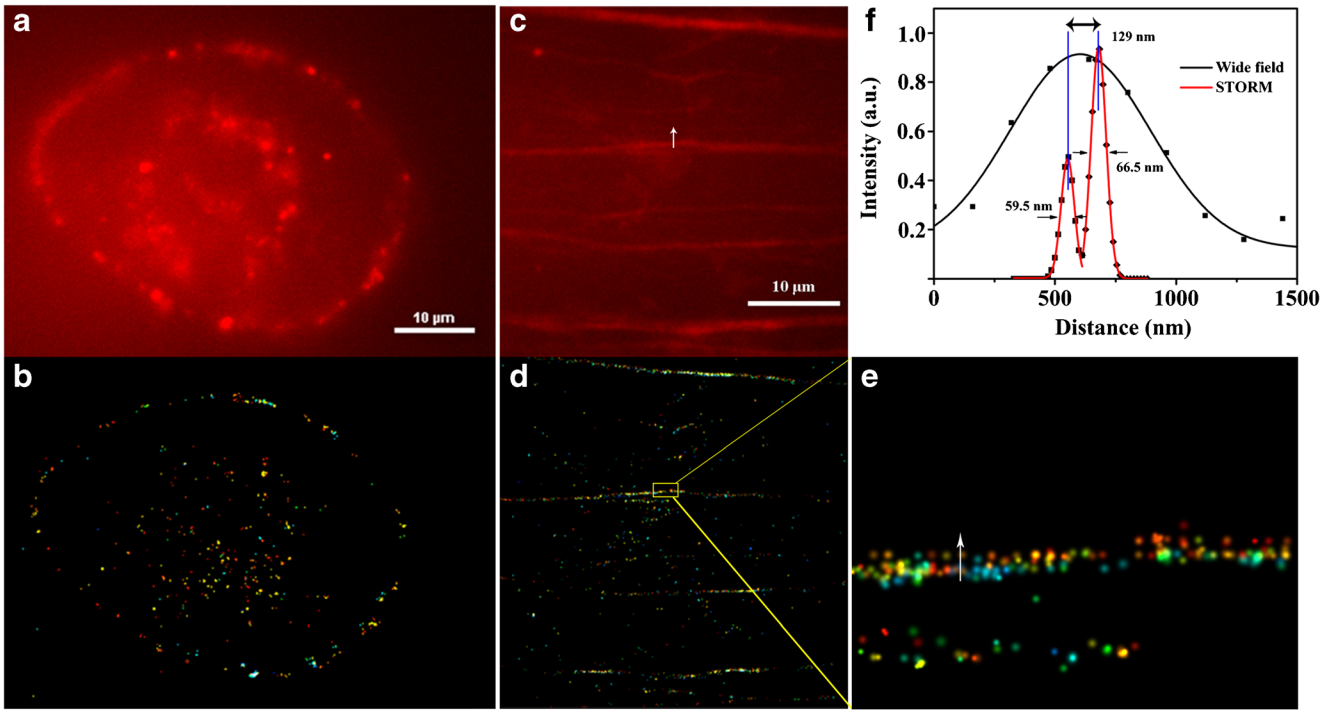

Fig. 8 **a** Wide-field and (**b**) reconstructed pseudocolor STORM image of N-CDs-labeled HeLa cells. **c** Wide-field imaging of DNA fibers and the corresponding pseudocolor STORM pattern (**d**). **e** The magnified image of the boxed region in panel d. **f** The intensity profiles of the white arrows in panel c and e

improvement than that of the wide-field image (Fig. 8f). In addition, Fig. 8e shows two clear DNA strands of DNA fibers, ~129 nm apart with a resolution down to ~59.5 nm, which is blurry and indistinguishable in the original image. It is noticeable that no external chemicals are needed to activate photoswitching in the abovementioned process of super-resolution imaging. On the basis of the above study, we can draw the conclusion that the N-CDs showed substantial promise for super-resolution imaging. Although CDs have been widely used in various sensing systems and imaging, there are still some issues that need to be addressed, for example, the poor reproducibility in size and quantum yield, difficulty of synthesizing CDs with accurately controlled structures, and the origin of their fluorescence. It is also unclear how the heteroatoms change the optical properties, etc. Further exploration is still needed.

Conclusion

A sensitive curcumin detection platform has been developed using N-doped CDs. Considering the remarkable fluorescence properties and good biocompatibility, N-CDs were also employed for fluorescent ink and bioimaging. Single-particle study indicated that the N-CDs exhibited strong photostability and fluorescence blinking. On the basis of that, we successfully achieved STORM images of N-CDs-labeled cells and DNA fibers with a resolution down to ~59.5 nm (fwhm). Effective image resolution is not only related with the brightness and photostability of the probes but also with the size of the fluorescent labels. Compared with some reported dyes and semiconductor quantum dots, N-CDs are less toxic alternatives with small particle size (~3 nm), which makes them more suitable for fine structures analysis of organisms in various super-resolution techniques, not restricted to STORM. Admittedly, further exploration is needed to tailor the N-CDs for specific labeling. We foresee that, the solution of the non-specificity for N-CDs will undoubtedly bring a new leap forward in direct visualization of numerous intracellular events with super resolution and precision.

Acknowledgements This work was financially supported by the National Natural Science Foundation of China (No. 21708007 and No. 21277110) and Natural Science Foundation of Hunan Province (No. 2018JJ3030). The authors would also like to thank Mr. Zhou Chunyuan for assistance in super-resolution microscopy data.

Compliance with ethical standards The author(s) declare that they have no competing interests.

Ethical approval All procedures performed in our studies were in accordance with the guidelines of the National Institute of Health, China, and approved by the Institutional Ethical Committee (IEC) of Hunan

University. We also obtained informed consent for any experimentation with human urine samples.

References

1. Abbe E (1873) Beiträge zur Theorie des Mikroskops und der mikroskopischen Wahrnehmung. Arch Mikroskop Anat 9(1):413–418. https://doi.org/10.1007/bf02956173
2. Sahl SJ, Hell SW, Jakobs S (2017) Fluorescence nanoscopy in cell biology. Nat Rev Mol Cell Bio 18(11):685–701. https://doi.org/10.1038/nrm.2017.71
3. Betzig E, Patterson GH, Sougrat R, Lindwasser OW, Olenych S, Bonifacino JS, Davidson MW, Lippincott-Schwartz J, Hess HF (2006) Imaging intracellular fluorescent proteins at nanometer resolution. Science 313(5793):1642–1645. https://doi.org/10.1126/science.1127344
4. Bates M, Huang B, Dempsey GT, Zhuang X (2007) Multicolor super-resolution imaging with photo-switchable fluorescent probes. Science 317(5845):1749–1753. https://doi.org/10.1126/science.1146598
5. Wang Y, Fruhwirth G, Cai E, Ng T, Selvin PR (2013) 3D super-resolution imaging with blinking quantum dots. Nano Lett 13(11):5233–5241. https://doi.org/10.1021/nl4026665
6. Patterson GH, Lippincott-Schwartz J (2002) A photoactivatable GFP for selective photolabeling of proteins and cells. Science 297(5588):1873–1877. https://doi.org/10.1126/science.1074952
7. van de Linde S, Krstić I, Prisner T, Doose S, Heilemann M, Sauer M (2011) Photoinduced formation of reversible dye radicals and their impact on super-resolution imaging. Photochem Photobiol Sci 10(4):499–506. https://doi.org/10.1039/c0pp00317d
8. Reineck P, Francis A, Orth A, Lau DWM, Nixon-Luke RDV, Rastogi ID, Razali WAW, Cordina NM, Parker LM, Sreenivasan VKA (2016) Brightness and Photostability of emerging red and near-IR fluorescent nanomaterials for bioimaging. Adv Opt Mater 4(10):1549–1557. https://doi.org/10.1002/adom.201600212
9. Xu X, Ray R, Gu Y, Ploehn HJ, Gearheart L, Raker K, Scrivens WA (2004) Electrophoretic analysis and purification of fluorescent single-walled carbon nanotube fragments. J Am Chem Soc 126(40):12736–12737. https://doi.org/10.1021/ja040082h
10. Hu C, Li M, Qiu J, Sun YP (2019) Design and fabrication of carbon dots for energy conversion and storage. Chem Soc Rev 48(8):2315–2337. https://doi.org/10.1039/c8cs00750k
11. Wang Y, Xia Y (2019) Optical, electrochemical and catalytic methods for in-vitro diagnosis using carbonaceous nanoparticles: a review. Microchim Acta 186(1):50–75. https://doi.org/10.1007/s00604-018-3110-1
12. Wang X, Sun G, Routh P, Kim DH, Huang W, Chen P (2014) Heteroatom-doped graphene materials: syntheses, properties and applications. Chem Soc Rev 43(20):7067–7098. https://doi.org/10.1039/c4cs00141a
13. Zhou J, Zhou H, Tang J, Deng S, Yan F, Li W, Qu M (2017) Carbon dots doped with heteroatoms for fluorescent bioimaging: a review. Microchim Acta 184(2):343–368. https://doi.org/10.1007/s00604-016-2043-9
14. Park Y, Yoo J, Lim B, Kwon W, Rhee SW (2016) Improving the functionality of carbon nanodots: doping and surface functionalization. J Mater Chem A 4(30):11582–11603. https://doi.org/10.1039/c6ta04813g
15. Bu L, Peng J, Peng H, Liu S, Xiao H, Liu D, Pan Z, Chen Y, Chen F, He Y (2016) Fluorescent carbon dots for the sensitive detection of Cr(VI) in aqueous media and their application in test papers. RSC Adv 6(98):95469–95475. https://doi.org/10.1039/c6ra19977a
16. Zhou X, Zhao G, Tan X, Qian X, Zhang T, Gui J, Yang L, Xie X (2019) Nitrogen-doped carbon dots with high quantum yield for colorimetric and fluorometric detection of ferric ions and in a fluorescent ink. Microchim Acta 186(2):67–75. https://doi.org/10.1007/s00604-018-3176-9
17. Pirsaheb M, Mohammadi S, Salimi A, Payandeh M (2019) Functionalized fluorescent carbon nanostructures for targeted imaging of cancer cells: a review. Microchim Acta 186(4):231–250. https://doi.org/10.1007/s00604-019-3338-4
18. Chizhik AM, Stein S, Dekaliuk MO, Battle C, Li W, Huss A, Platen M, Schaap IA, Gregor I, Demchenko AP (2015) Super-resolution optical fluctuation bio-imaging with dual-color carbon nanodots. Nano Lett 16(1):237–242. https://doi.org/10.1021/acs.nanolett.5b03609
19. Heilemann M, van de Linde S, Mukherjee A, Sauer M (2009) Super-resolution imaging with small organic fluorophores. Angew Chem Int Ed 48(37):6903–6908. https://doi.org/10.1002/anie.200902073
20. Xu L, Fan H, Huang L, Xia J, Huang J, Li M, Ding H, Huang K, Li S (2017) Eosinophilic nitrogen-doped carbon dots derived from tribute chrysanthemum for label-free detection of Fe^{3+} ions and hydrazine. J Taiwan Inst Chem E 78:247–253. https://doi.org/10.1016/j.jtice.2017.06.011
21. Srivastava RM, Singh S, Dubey SK, Misra K, Khar A (2011) Immunomodulatory and therapeutic activity of curcumin. Int Immunopharmacol 11(3):331–341. https://doi.org/10.1016/j.intimp.2010.08.014
22. Merrick CJ, Jackson D, Diffley JF (2004) Visualization of altered replication dynamics after DNA damage in human cells. J Biol Chem 279(19):20067–20075. https://doi.org/10.1074/jbc.M400022200
23. Biedermann LB, Bolen ML, Capano MA (2009) Insights into few-layer epitaxial graphene growth on 4 H-SiC (0001¯) substrates from STM studies. Phys Rev B 79(12):125411–125410. https://doi.org/10.1103/PhysRevB.79.125411
24. Pan D, Zhang J, Li Z, Wu M (2010) Hydrothermal route for cutting graphene sheets into blue-luminescent graphene quantum dots. Adv Mater 22(6):734–738. https://doi.org/10.1002/adma.200902825
25. Tang L, Ji R, Cao X, Lin J, Jiang H, Li X, Teng KS, Luk CM, Zeng S, Hao J (2012) Deep ultraviolet photoluminescence of water-soluble self-passivated graphene quantum dots. ACS Nano 6(6):5102–5110. https://doi.org/10.1021/nn300760g
26. Liang Q, Ma W, Shi Y, Li Z, Yang X (2013) Easy synthesis of highly fluorescent carbon quantum dots from gelatin and their luminescent properties and applications. Carbon 60(12):421–428. https://doi.org/10.1016/j.carbon.2013.04.055
27. Dong Y, Pang H, Yang HB, Guo C, Shao J, Chi Y, Li CM, Yu T (2013) Carbon-based dots co-doped with nitrogen and sulfur for high quantum yield and excitation-independent emission. Angew Chem Int Ed 125(30):7954–7958. https://doi.org/10.1002/ange.201301114
28. Zhou H, Beevers CS, Huang S (2011) The targets of curcumin. Curr Drug Targets 12(3):332–347. https://doi.org/10.2174/138945011794815356
29. Zhang Q, Chen B, Zou H, Li Y, Huang C (2018) Inner filter with carbon quantum dots: a selective sensing platform for detection of hematin in human red cells. Biosens Bioelectron 100:148–154. https://doi.org/10.1016/j.bios.2017.08.049
30. Lakowicz JR (1999) Principles of fluorescence spectroscopy, 2nd edn. Kluwer Academic, New York
31. Xu H, Yu DH, Liu LL, Yan PH, Yue ZY (2010) Small molecular glasses based on multiposition encapsulated phenyl benzimidazole iridium(III) complexes: toward efficient solution-processable host-

free electrophosphorescent diodes. J Phys Chem B 114(1):141–150. https://doi.org/10.1021/jp909297d

32. Zhang H, Chen Y, Liang M, Xu L, Qi S, Chen H, Chen X (2014) Solid-phase synthesis of highly fluorescent nitrogen-doped carbon dots for sensitive and selective probing ferric ions in living cells. Anal Chem 86(19):9846–9852. https://doi.org/10.1021/ac502446m
33. Verma NC, Rao C, Nandi CK (2018) Nitrogen-doped biocompatible carbon dot as a fluorescent probe for STORM nanoscopy. J Phys Chem C 122(8):4704–4709. https://doi.org/10.1021/acs.jpcc.7b12773
34. Das SK, Liu Y, Yeom S, Kim DY, Richards CI (2014) Single-particle fluorescence intensity fluctuations of carbon nanodots. Nano Lett 14(2):620–625. https://doi.org/10.1021/nl403820m